

# CFD Numerical Study of a New Crossed Inverse Z Flow Field for PEMFC

Fayi Yan\*, Jian Yao, Xuejian Pei

School of Mechanical and Electronic Engineering, Shandong Jianzhu University, Jinan 250101, Shandong, PR China

\*E-mail: [915281448@qq.com](mailto:915281448@qq.com)

*Received:* 3 March 2022 / *Accepted:* 21 April 2022 / *Published:* 6 June 2022

---

Proton exchange membrane fuel cells (PEMFCs) are used to convert chemical energy into electrical energy. The bipolar plate is an important part of PEMFC. The flow field structure can be found in the bipolar plate, and an appropriate flow field structure has a crucial influence on the performance of fuel cells. In this paper, a new inlet was proposed, which is located in the center of the plate crossing the inverse Z flow field and four main channels connected with an air inlet. Each main channel connects simultaneously multiple branch channels, the mutual not interference between each branch channels, and the reaction gas caused by the flow of the main branch flow channel, which reduces the uneven distribution of reactants in conventional flow fields. Based on CFD simulation analysis, the new flow field has the best output performance when the rib width ratio and inlet/outlet area ratio are both 2/1. Results of this study provide a new idea for improving the performance of PEMFC.

---

**Keywords:** Proton exchange membrane fuel cell (PEMFC); Cross inverse Z flow field; Uniform convergent flow channel; CFD simulation analysis

## 1. INTRODUCTION

Proton exchange membrane fuel cells (PEMFCs) can convert chemical energy into electric energy. At present, it is widely used in environmental protection because of its high energy conversion efficiency and clean and efficient characteristics [1–4]. However, some PEMFCs still have low current transmission capacity, and they can be easily flooded under high current density. This shortcoming will affect the commercialization of fuel cells. In general, a PEMFC cathode generally oxygen (air) as an oxidant and anode hydrogen as a reducing agent, and the bipolar plate is an important components of fuel cells. The performance of fuel cells depends on the bipolar plate, and the weight of the bipolar plate accounts for about 80% of the total weight of the fuel cell stack. The flow field structure can be found in the bipolar plate, which directly affects the diffusion and mass transfer of reaction gas to the anode

and cathode gas diffusion layer (GDL), and then the electrochemical reaction. The performance of PEMFC is greatly affected by the flow field channel structure [5–13]. Considerable research aims to improve the flow field structure and the performance of fuel cells.

Flow field type and channel rib width ratio are important factors affecting the performance of PEMFC. Kim [14] improved the performance of blast PEMFC by reducing the size of the cathode flow channel and changing the operating parameters of the whole flow field. Shimpalee and Muthukumar conducted numerical analysis on the serpentine flow channel by changing the rib width ratio and the number of flow channels respectively [15,16]. The results show that changing the flow channel size can effectively improve the working efficiency of fuel cells. In addition, changing the flow field layout can improve the performance of PEMFC. Cooper [17] conducted an experimental analysis on parallel flow field and interdigitated flow field, and found that the factors affecting the chemical performance of different types of flow field. The results show that stoichiometric ratio can greatly affect the flow field performance of fingered flow field greatly, and an appropriate rib width ratio could remarkably improve the power density of parallel flow field.

Changing the size of the internal space of the flow channel can also improve the performance of PEMFC. Heidary [18] improved the performance of PEMFC by embedding rectangular blocks on bipolar plates to affect the cross-sectional area of the flow channel, whereas Perng [19] changed the cross-sectional area of the flow channel by installing baffles. Wang [20] conducted gradient treatment on the flow channel of serpentine flow field fuel cell, and the results show that the indented flow field can effectively alleviate water aggregation phenomenon inside the flow field, thereby improving the working efficiency of fuel cells. Korkischko [21] analyzed a variety of flow channels with different cross-section shapes and found that the current density distribution of the inverted trapezoidal flow channel was uniform, Moreover, the power density was markedly increased compared with the rectangular flow channel.

Appropriate flow field structure and size can improve the electrochemical performance of fuel cells [22–26]. Based on the abovementioned literature, considerable structural transformation, numerical calculation and performance research have been conducted on PEMFC flow field structure, but some shortcomings are still found. In particular, the research on the central inlet flow field primarily focuses on the radial flow field and the spiral flow field [27], but these two types still have some shortcomings that are difficult to solve. Based on the abovementioned analysis, in this paper, a cross inverse Z flow field with a square plate containing a central inlet was proposed. Simulation analysis of the new flow field was performed using COMSOL Multiphysics. The width of channel/width of rib (rib width ratio) and flow channel section area were selected as the research focus, and multiple flow channel models were established. The advantages and disadvantages of different flow channel fuel cells in oxygen concentration distribution and water concentration distribution were compared to obtain reliable results.

## **2. MODEL DESCRIPTION**

### *2.1. Geometric Model*

The PEMFC is composed of a bipolar plate, GDL, polar catalytic layer (CL), proton exchange membrane, and other structures [28–30]. In this paper, the edge inlet is not adopted as the traditional

flow field, but the air inlet is set in the center of the square plate. The flow field adopts the arrangement of the cross inverse Z flow channel. The four main roads are equipped with multiple branches, which can effectively prevent the slow oxygen supply at the outlet end. In this structure, the rib width ratio and inlet/outlet area ratio are set as key variables. The specific geometric model is shown in Figure 1, and the geometric parameters are shown in Table 1.

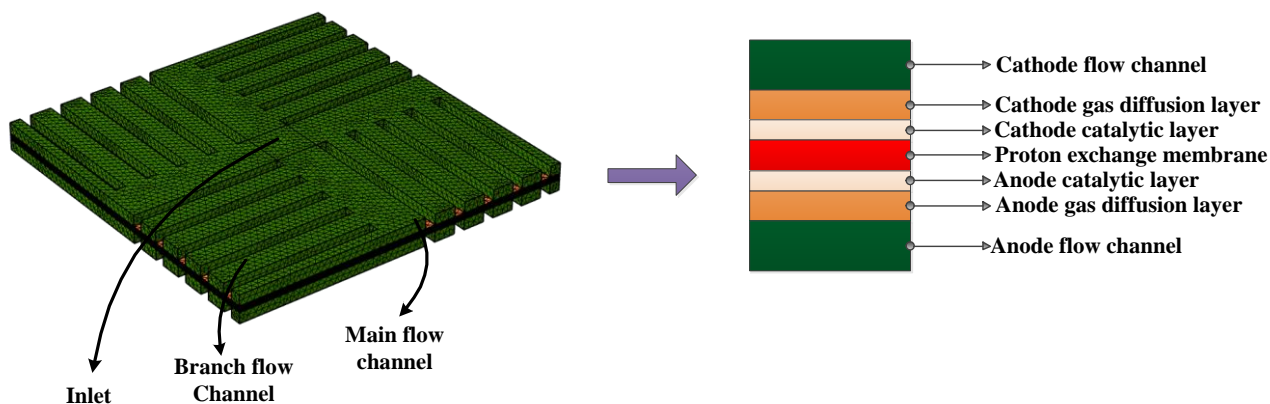


Figure 1. New geometric model of flow field

Table 1. Main geometric parameters

Parameter	Value	Unit
Thickness of the membrane	0.183	mm
Floor height	1	mm
Floor width	1	mm
GDL thickness	0.19	mm
Porous electrode thickness	0.015	mm
Main channel width	4	mm
Plate length	32	mm
Number of main channels	4	

### 2.2 Control equations

This paper uses the “Reactive Flow, Concentrated Matter” interface in COMSOL to describe the flow and mass transfer modeling and solve for the velocity and pressure of the fluid, as well as the mass fraction of oxygen, water, and nitrogen in the gas stream.

(1) A single substance follows the law of conservation of mass, and the change in the total amount of matter in any region is equal to the change in mass from the boundary into or the sum of the masses leaving. The conservation of mass equation is calculated as follows:

$$\frac{\partial(\varepsilon\rho)}{\partial t} + \nabla \cdot (\varepsilon\rho\vec{u}) = S_m \tag{1}$$

where,  $\rho$  indicates the density;  $\varepsilon$  indicates the porosity;  $S_m$  indicates the quality source term;  $\vec{u}$  indicates the velocity vector, and  $\nabla$  indicates the calculator. In Equation (1), the first term represents the transient term, which indicates the amount of mass accumulated over time. The second term represents the change in mass flux.

For  $S_m$ , different computational domains require different solution formulas, in areas such as the cathode GDL and cathode flow channel,  $S_m = 0$ . The cathodic CL and the anodic CL, where the chemical reaction occurs, are calculated as follows:

$$S_{ma} = S_{H_2} = -\frac{M_{H_2}}{2F} i_a \quad (2)$$

$$S_{mc} = S_{H_2O} + S_{O_2} = \frac{M_{H_2O}}{2F} i_c - \frac{M_{O_2}}{4F} i_c \quad (3)$$

where  $M$  denotes the molar mass;  $F$  denotes Faraday's constant, and  $i$  denotes the exchange current density, and  $S_{ma}$  and  $S_{mc}$  denote the source terms of the positive and negative masses, respectively.

(2) The conservation of momentum represents the pressure gradient inside the porous medium because of the loss of momentum in the flow, which is calculated as follows:

$$\frac{\partial(\varepsilon\rho)}{\partial t} + \nabla \cdot (\varepsilon\rho\bar{u}) = -\varepsilon\nabla P + \nabla \cdot (\varepsilon\mu\nabla\bar{u}) + S_u \quad (4)$$

where  $P$  denotes the pressure;  $\mu$  denotes the kinetic viscosity, and  $S_u$  denotes the power source term. In the fuel cell flow field,  $\varepsilon = 1$ ,  $S_u = 1$ , and in the cathode GDL and cathode CL, the viscous and inertial forces have less influence on other components because of the low permeation velocity of each component. The momentum conservation equation can be directly simplified by Darcy's law, which is presented as follows:

$$S_u = -\frac{K_p}{\mu} \nabla P \quad (5)$$

where  $K_p$  denotes the permeability of porous media.

(3) The equation of energy conservation in either region of the PEMFC can be expressed as follows:

$$\frac{\partial(\varepsilon\rho C_p T)}{\partial t} + \nabla \cdot (\varepsilon\rho C_p \bar{u} T) = \nabla \cdot (K^{\text{eff}} \nabla T) + S_Q \quad (6)$$

where  $C_p$  is the constant pressure specific heat;  $T$  is the temperature;  $k$  is the thermal conductivity, and the subscript eff indicates the effectiveness of the porous medium.  $S_Q$  indicates the energy source term.

The source term can be expressed as follows:

$$S_Q = j^2 R_{ohm} + \beta \dot{m}_{H_2O} h_{rxn} + r_w h_L + j_{a,c} \eta \quad (7)$$

where  $j$  is the current density;  $\beta$  represents the ratio of energy conversion from chemical to thermal energy.  $\dot{m}_{H_2O}$  represents the rate of gaseous water production;  $h_{rxn}$  is the enthalpy of reaction;  $r_w$  is the rate of phase change of water;  $h_L$  represents the enthalpy of phase change of water, and  $\eta$  represents the overpotential.

(4) The component conservation equation is presented as follows:

$$\frac{\partial(\varepsilon\rho)}{\partial t} + \nabla \cdot (\varepsilon\rho\bar{u}) = \nabla \cdot (D_K^{\text{eff}} \nabla \rho) + S_K \quad (8)$$

where  $D_K^{\text{eff}}$  is the effective diffusion coefficient of each component, and  $S_K$  is the source term.

(5) The current transport can be described on the basis of the conservation of charge in a PEMFC, including the solid phase potential and membrane phase potential, and the controlling equations and source terms for the proton and electron transport are calculated as follows:

$$\nabla \bullet (\delta_{sol} \nabla \phi_{sol}) + R_{sol} = 0 \quad (9)$$

$$\nabla \bullet (\delta_{mem} \nabla \phi_{mem}) + R_{mem} = 0 \quad (10)$$

where  $\delta$  is the conductivity;  $R$  is the exchange current density;  $\phi$  is the phase voltage, and *sol* and *mem* denote the solid phase and membrane phase, respectively.

(6) The water content saturation equation is presented as follows:

$$\frac{\partial(\varepsilon \rho_1 s)}{\partial t} + \nabla \left[ \rho_1 \frac{K_s}{\mu_1} \frac{dP_c}{d_s} \nabla_s \right] = r_w \quad (11)$$

where  $\varepsilon$  is the porosity;  $\rho_1$  is the liquid water density;  $\mu_1$  is the liquid water viscosity;  $s$  indicates water saturation;  $r_w$  indicates the condensation rate, and  $P_c$  indicates the capillary pressure. In this paper, the working temperature is set as  $70 \text{ }^\circ\text{C} < 90 \text{ }^\circ\text{C}$ ; thus, the capillary pressure is calculated as follows:

$$P_c = \frac{\sigma \cos \theta_c}{\left(\frac{K}{\varepsilon}\right)^{0.5}} \left[ 1.147(1-s) - 2.12(1-s)^2 + 1.263(1-s)^3 \right] \quad (12)$$

where  $\sigma$  is the surface tension;  $\theta_c$  is the contact angle, and  $K$  is the absolute permeability.

### 2.3. Model assumptions

1. The fuel cell operates under stable conditions, and the gravity is ignored.
2. The flow state inside the fuel cell is laminar flow.
3. The proton exchange membrane is electrically insulated.
4. All gases are incompressible ideal gases.
5. All porous media are isotropic and homogeneous.
6. Symmetric boundary conditions are applied along the long edge of GDL and GDE (gas diffusion electrode). The slip-free boundary condition is applied to all other wall boundaries.

### 2.4 Model parameters

The main function of fuel cell flow field is to provide gas necessary for reaction and discharge liquid water and reactants without chemical reaction. Different types of flow field structure will have a great impact on the performance of the battery. Table 2 shows the material parameters used in the calculation process and operating parameters of fuel cells.

**Table 2.** Basic structural parameters and physical parameters

Parameter	Value	Unit
Battery temperature	80+273.15	<i>K</i>
GDL porosity	0.4	
GDL permeability	1e-13	<i>m</i> <sup>2</sup>
The reference pressure	101e3	<i>Pa</i>
Anode inlet velocity	0.3	<i>m/s</i>
Cathode inlet velocity	0.3	<i>m/s</i>
CL porosity	0.3	
The binary diffusion coefficient of H <sub>2</sub> -H <sub>2</sub> O	0.00011684	<i>m</i> <sup>2</sup> / <i>s</i>

The binary diffusion coefficient of N <sub>2</sub> -H <sub>2</sub> O	0.000032682	m <sup>2</sup> /s
The binary diffusion coefficient of O <sub>2</sub> -H <sub>2</sub> O	0.000035807	m <sup>2</sup> /s
Binary diffusion coefficient of O <sub>2</sub> -N <sub>2</sub>	0.000030466	m <sup>2</sup> /s
CL permeability	2e-14	m <sup>2</sup>
Membrane conductivity	9	S/m
Anode dynamic viscosity	1.19E-5	Pa·s
Cathodic dynamic viscosity	2.46E-5	Pa·s
Imported hydrogen mass fraction (anode)	0.743	
Inlet water mass fraction (cathode)	0.023	
Imported oxygen mass fraction (cathode)	0.228	

### 2.5 Validation of model rationality

Xie [31] designed and processed a fuel cell bipolar monomer model and measured a group of polarization curve data. Under the same external conditions such as intake flow rate and size, the same 3D model was established and simulated. The results obtained are shown in Figure 2. The deviation between the experimental value and simulation value is less than 5%; thus, the simulation can be considered reasonable, and the numerical model can be extended to other structures.

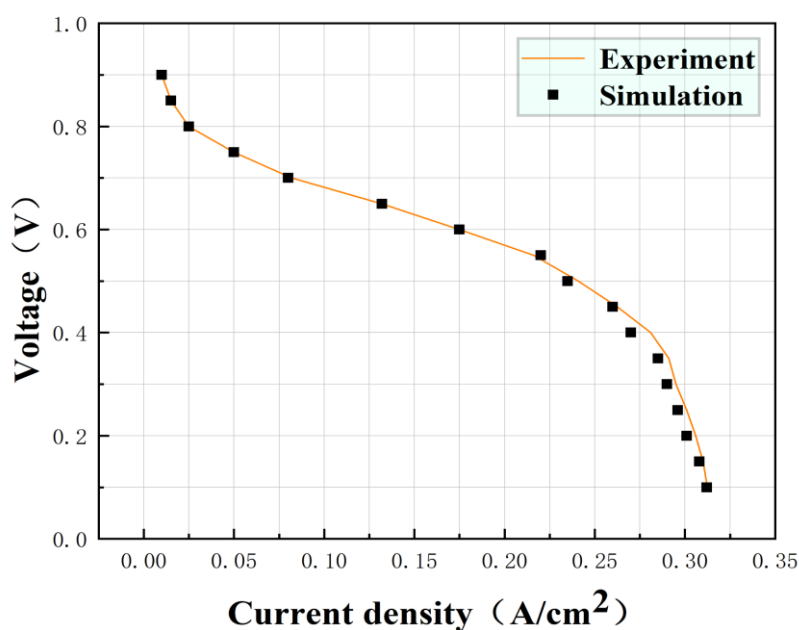


Figure 2. Comparison between simulation results and experimental data

### 3. RESULT AND DISCUSSION

The oxygen concentration distribution, water concentration distribution, and pressure drop of PEMFC were compared and analyzed to understand the influence of different flow channels on fuel cell performance, and the advantages and disadvantages of different transformation types could be clearly understood from the results.

### 3.1 Different rib width ratios

Five types of PEMFC derivatives are included, and the ratio of channel width to rib width is style 1 (1/2), style 2 (1/1), style 3 (2/1), style 4 (3/1), and style 5 (4/1). The flow field of the five styles are all center inlet, and the square inlet is adopted. The side length of the square plate is 32 mm. The specific classification is shown in Table 3.

**Table 3.** Different width of ribs and channels

Style	Rib width(mm)	Flow channel width(mm)	Rib width ratio
style1	1	0.5	1/2
style2	1	1	1/1
style3	1	2	2/1
style4	1	3	3/1
style5	1	4	4/1

#### 3.1.1. Impact on PEMFC performance

A membrane electrode assembly (MEA) is the core component of fuel cells, and the flow field can reasonably distribute the reaction gas; thus, the permeability of the reaction gas is stronger when it reaches the MEA. The right rib width ratio can effectively induce the reaction gas flow direction. However, the rib is too wide to make a narrow channel area, the reaction gas is in short supply, and the chemical reaction has low efficiency. If the rib plate is too narrow, then the reaction gas flow speed will be slow; the resistance will increase, and the pressure will be too large. Therefore, selecting the appropriate rib width ratio plays a great role in improving the performance of PEMFC.

Figure 3 shows the polarization curves and power density curves of PEMFC with different rib width ratios. As shown in the figure, under low current density, the polarization curves of different flow fields are highly consistent with the power density curves, and the output performance of the fuel cell is similar. With the increase of current density, the performance curves show evident differences. Therefore, with the increases of rib width ratio and after the first increase in power density value change trend of decrease, the rib width ratio is 1 (Style 2), and it has the largest PEMFC power density value. When the rib width ratio is greater than 1, along with the decrease of the rib width ratio, the limiting current density and power density of PEMFC significantly decreased, and the rib width ratio is less than 1, Fuel cells show the worst output characteristic, with the maximum power output of Style 1 being lower than other types.

Notably, Xie proposed a new three-dimensional radial flow field with a central inlet, and obtained the flow channel width value under the optimal condition [31]. Compared with Xie's design, changing the channel width of the flow field in this paper has a more evident effect on improving the output power of fuel cells. Moreover, although the initial air intake flow set in this paper is low, the maximum power density of Styles 2–5 is still higher than that of Xie (0.12 W/cm<sup>2</sup>), which indicates that this model is more advantageous in improving the output power of PEMFC.

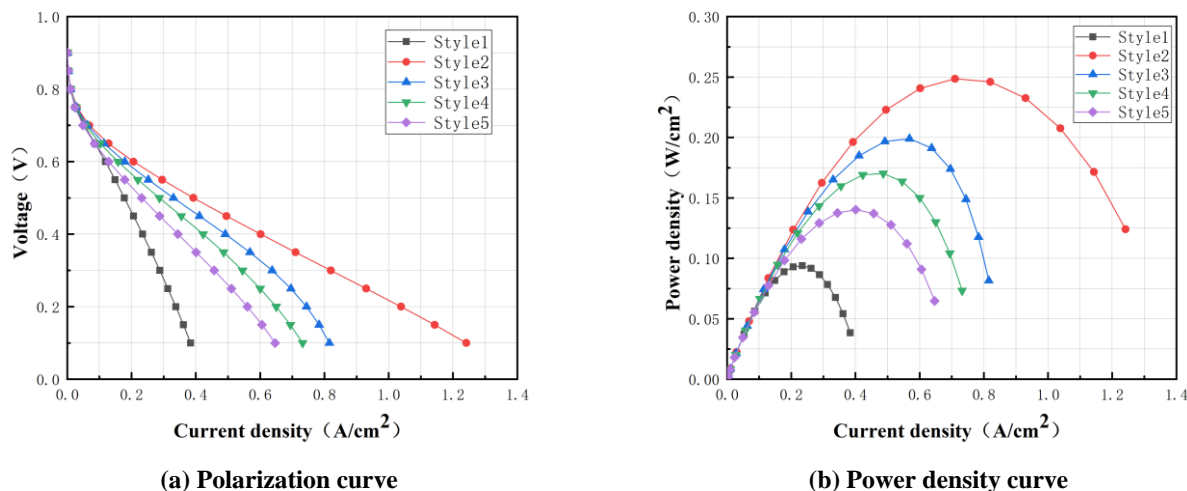


**Figure 3.** Performance curves of PEMFC with different rib width ratios

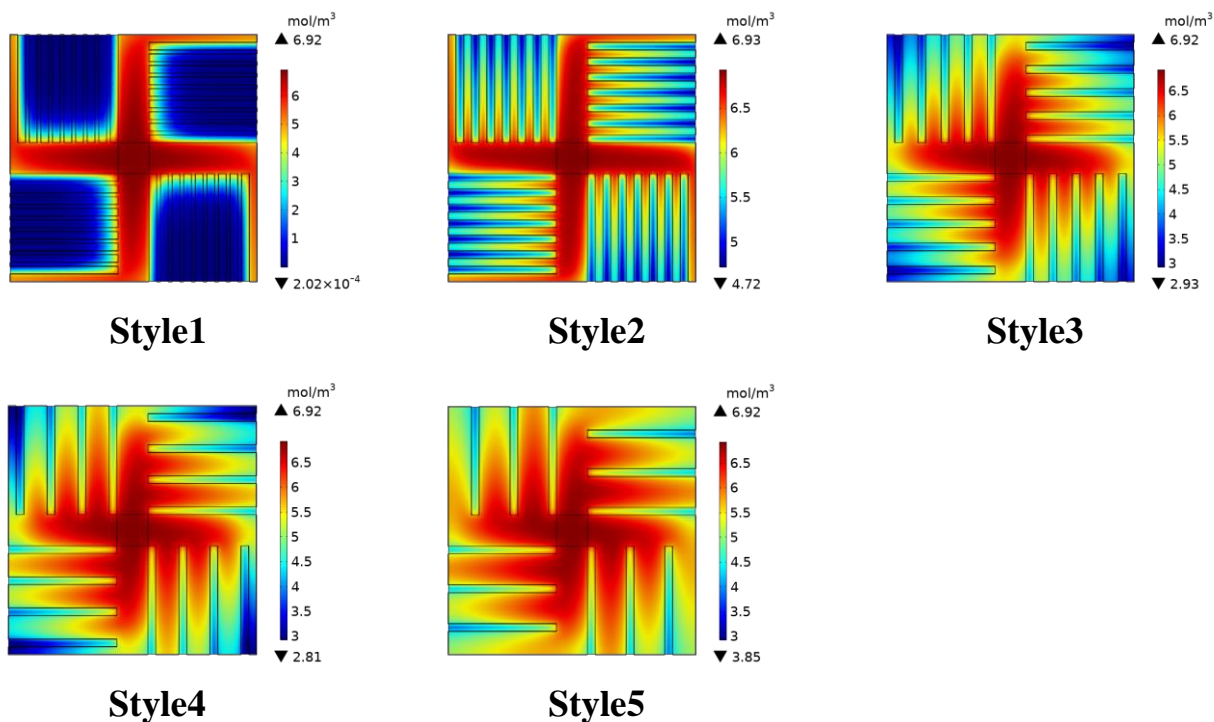
### 3.1.2. Influence on oxygen concentration distribution in the GDL/CL layer

Figure 4 shows the voltage under the condition of 0.55 V, different rib width ratios fuel cell layer of GDL/CL oxygen concentration distribution. As shown in the diagram, the inlet located in the center of the plate can make the whole flow field of the reactant concentration distribution more homogeneous to cross inverse Z flow field, and under the four main flow channels oxygen density all maintain at a high level. Relative to the main channel, the oxygen concentration level at the corresponding position of each branch decreases remarkably, which is due to the constant chemical reaction of oxygen consumption during the transfer process. The farther the air inlet, the lower the oxygen concentration value.

Figure 4 shows different oxygen concentration distributions of different types of flow field. Compared with other types, Style 1 oxygen concentration is not uniformly distributed probably because a narrow channel can reduce the ability of oxygen to pass. Higher pressure in the main channel leads to high oxygen concentration at the corresponding position of the outermost channel, within the branch flow channel caused by blocked rib low oxygen concentration. Compared with Style 1, the oxygen concentration distribution of Styles 2–5 is remarkably improved, and the oxygen distribution of Style 2 is the most uniform. Except for the flow channel near the outlet and the outermost flow channel, most of the flow channel areas of Style 3 have with sufficient oxygen supply, because a wide flow channel can improve the ability of oxygen to pass. The gas pressure in the outermost flow channel is low, but the reaction gas flow at the entrance of the flow field is limited. When it reaches the farthest end of the flow field, it is affected by the gas movement speed and reaction consumption, resulting in insufficient oxygen supply in some areas.

At 0.65 V, Xie obtained the optimal solution for the flow channel width, in which the oxygen concentration difference of the GDL/CL layer is approximately 6.5 mol/m<sup>3</sup>. Under similar conditions, the oxygen concentration difference of Styles 2–3 was kept below 2 mol/m<sup>3</sup>. Furthermore, compared with the serpentine flow channel proposed by Wang [32], the oxygen concentration difference is almost identical under similar conditions. However, based on the overall distribution, the high oxygen concentration region of Styles 2–3 is significantly larger. This result indicates that the new flow field

adopted in this paper can improve the distribution uniformity of oxygen concentration in the GDL/CL layer.



**Figure 4.** The oxygen concentration distribution of different styles in the GDL/CL layer

### 3.1.3 Influence on membrane water content distribution

At 100 °C, the reaction of water in liquid form exists in PEMFC. The chemical reaction of electronic conduction uses water as medium, and the water content of membrane and the flow channel directly impact on the output of the fuel cell performance and service life of membrane. In addition, excessively high moisture content can cause “flooding” phenomenon, which hinders the effective diffusion of reaction gas. If the water content in the membrane is too low, then membrane will dry and crack, which not only affects the service life of the membrane, but also reduces the chemical reaction rate. Moreover, when the water content in the membrane is very low, then artificial humidification through external action is needed to ensure normal reaction.

Figure 5 shows the membrane water content distribution of flow channel PEMFC with different rib width ratios at 0.55 V. As shown in the figure, the membrane water content under the main flow channel is the lowest, and the corresponding membrane water content of each branch flow channel area increases with the increase of the distance from the air inlet. Based on the five flow fields, Style 1 has the highest membrane water content. Notably, under similar conditions, the difference of water concentration in the membrane of serpentine runner proposed by Wang is also increased by 57.89% compared with Style 3 [32]. However, excessive water accumulation results in poor chemical properties of the flow field. On the contrary, Style 2 has a uniform water content, but it is relatively low. Compared with Style 3, the concentration of water in the Style 2 membrane decreased by 60.29%, which is not conducive to the rapid conduction of electrons. Compared with Style 5 the water content in the Styles

3–4 membrane is similar and evenly distributed, indicating that the narrow or wide channel width is not conducive to the rational distribution of liquid water in the membrane.

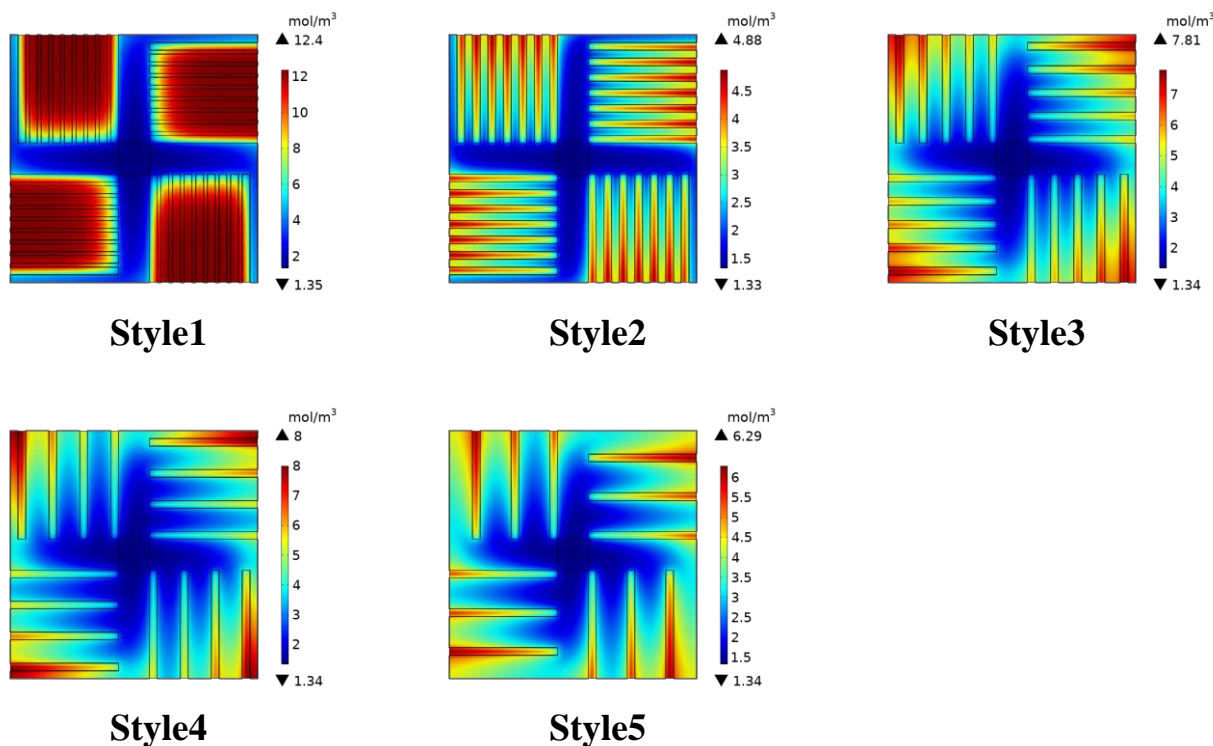


**Figure 5.** The water content distribution of different styles in the membrane

### 3.1.4 Influence on water content distribution of the flow channel

The water content of the flow channel has an important influence on the output performance of PEMFC. The high water content of the flow channel will lead to poor reaction gas transmission and high pressure in the flow field. Figure 6 shows the water content distribution diagram of the flow channel of PEMFC with different rib width ratios at 0.55 V. As shown in the figure the farther the air inlet, the higher the water content in the flow channel. This result is primarily due to the decrease in oxygen movement rate, which causes the inability of the flow channel to carry the liquid water produced by chemical reactions out of the flow field in time. In addition, the movement rate of reaction gas can be effectively increased by using the uniform convergent branch flow channel, which will be mentioned in the subsequent structural changes of the branch flow channel. The comparison among the five types of PEMFC derivatives shows that the average water content of Style 2 is the lowest, whereas that of Style 3 is higher than that of Style 5 but still lower than that of Style 4 and Style 1. The distribution of water content in the flow channel shows a reverse trend with the distribution of oxygen concentration at the GDL/CL layer, indicating that excessive water accumulation in the flow channel will hinder the normal diffusion of oxygen.

Lian compared the water removal effects of the cathode channel of different types of flow fields [33]. The difference of water concentration in the cathode channel of different types of flow fields was compared with Style 3 to determine the advantages of the new flow field in the water removal ability of the cathode channel. The results are shown in Figure 7. The figure shows that under similar conditions,

the water concentration difference of Style 3 (2.7 mol/m<sup>3</sup>) is lower than that of all traditional flow fields. Therefore, the new flow field has a remarkable water removal effect.

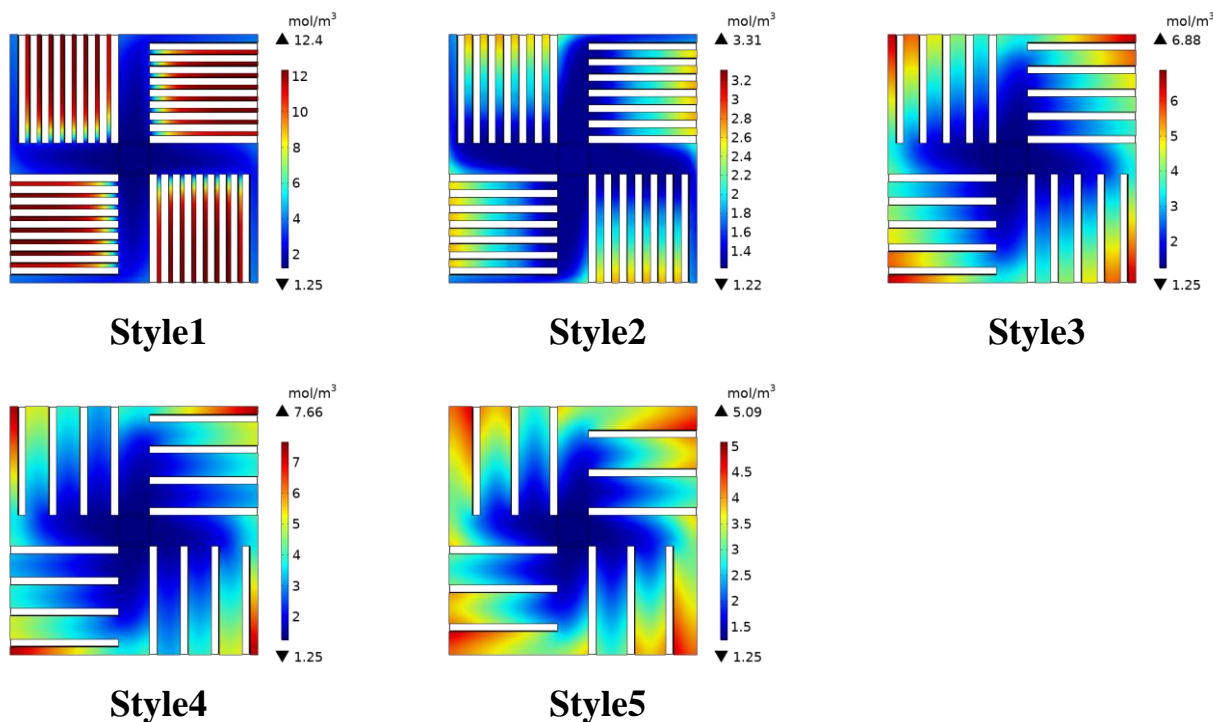


Figure 6. The water content distribution of different styles in the flow channel

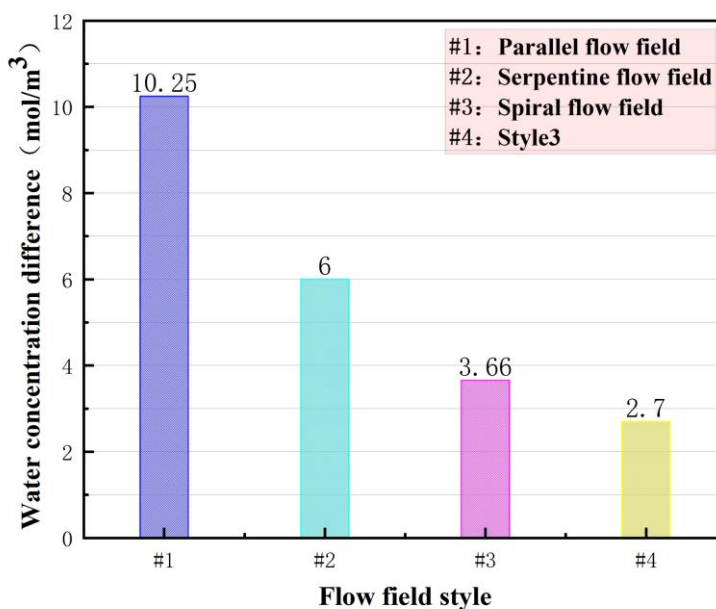
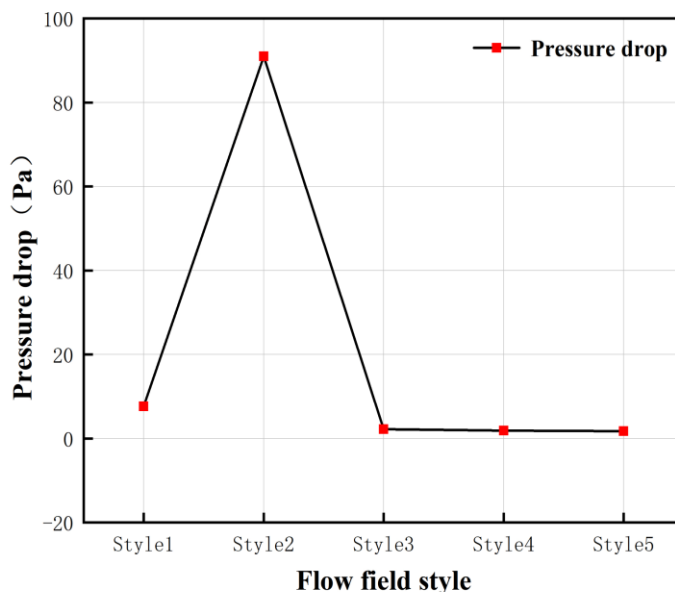


Figure 7. Difference of water concentration in different styles of flow field

### 3.1.5 Influence on pressure drop of the cathode channel

Pressure drop is also an important reference index to measure the flow channel design of PEMFC. If the flow channel pressure drop is too large, then the pump power required to transport the reaction gas will be relatively higher, and the overall cost of the fuel cell power output will also increase. Figure 8

shows the pressure drop of the cathode flow channel of PEMFC with different rib width ratios. As shown in the figure, the pressure drop of Style 1 and Style 2 is evidently higher than that of other types. Although Style 2 has the largest power density, the pressure drop is too large to make it the first option of new flow field. Jang [34] compared the pressure drop values of parallel flow field, serpentine flow field, and Z-type flow field, but under similar conditions, even the parallel flow field with the smallest pressure drop value was higher than Style 3. Therefore, Style 3 (rib width ratio is 2/1) has the best overall performance.



**Figure 8.** Cathode flow channel pressure drop of PEMFC with different rib width ratios

### 3.2 Different inlet/outlet area ratios

Based on the abovementioned analysis, Style 3 (rib width ratio is 2/1) has the best comprehensive performance compared with other types of flow channels. A uniform convergent design of flow channel branches is adopted to improve the output characteristics of Style 3. The specific classification method is shown in Table 4.

**Table 4.** Different inlet/outlet area ratios of PEMFC channel branches

Flow channel style	Rib width ratio	Branch inlet/outlet area ratio
Style3	2/1	1/1
Style6	2/1	2/1
Style7	2/1	2.5/1
Style8	2/1	5/1
Style9	2/1	5/7

### 3.2.1 Impact on PEMFC performance

Figure 9 shows the polarization curves and power density curves of different inlet/outlet area ratios of PEMFC branch channels. As shown in the figure, the performance of Style 8 decreases remarkably, and the limiting current density values and maximum power density values are relatively small compared with other styles, which indicates that too small outlet area will seriously reduce the output performance of new flow field PEMFC. In addition, the divergent flow field has a certain disadvantage compared with the convergent flow field. Although the flow field area of the increasing flow field increases, the wider flow channel size reduces the movement rate of reaction gas, resulting in poor drainage in the flow channel.

During convergence, as a homogeneous type of flow field, the output power of PEMFC decreases with the increase of the inlet/outlet area ratio. In addition, when the style of flow field branch outlet area is less than the entrance area, the reaction gas caused by the decrease of the channel interior space increases the gas molecules and flow channel wall contact frequency, thereby improving the movement speed of the reaction gas. On the one hand, the increase of gas movement rate can improve the distribution uniformity of oxygen concentration. On the other hand, it can effectively remove the liquid water generated by the reaction [35]. Therefore, appropriately reducing the outlet area of the branch channel can improve the working efficiency of PEMFC.

The comparison between Style 6, which has the maximum power density among the five optimization styles, and Xie’s optimal model shows that the maximum power density ( $0.2 \text{ W/cm}^2$ ) of Style 6 increases by 33.33%. Compared with Style 3, the maximum power density of Style 6 is partially improved. Therefore, changing the inlet/outlet area ratio is an effective method to improve the output performance of PEMFC.

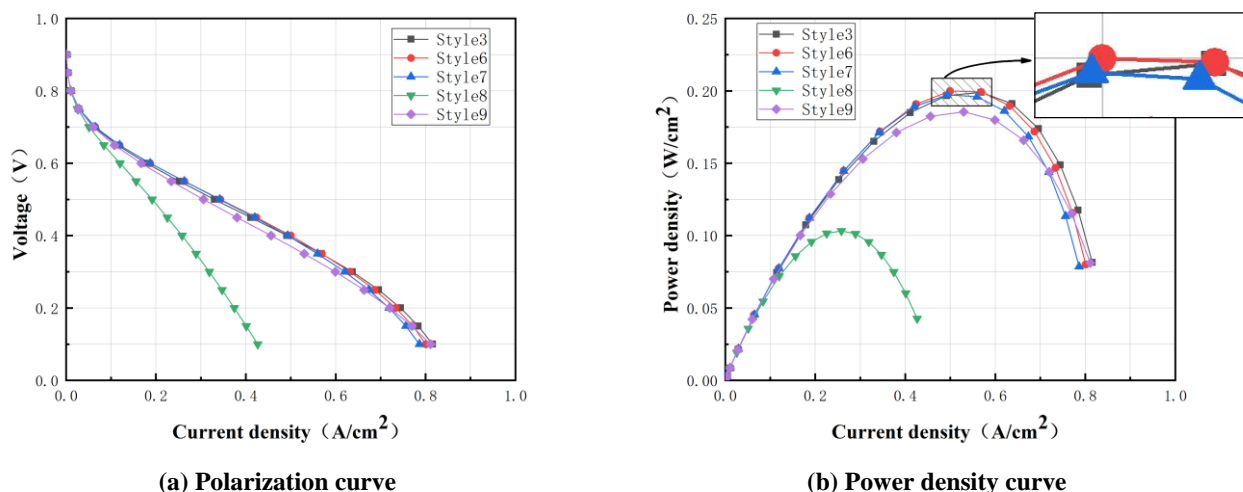


**Figure 9.** Performance curve of PEMFC with different inlet/outlet area ratios

### 3.2.2 Influence on oxygen concentration distribution in the GDL/CL layer

Figure 10 shows the oxygen concentration distribution of five different flow fields in the GDL/CL layer at 0.55 V. As shown in the figure, the uniform divergent flow field has the most uniform

oxygen concentration distribution, indicating that a relatively wide flow channel is conducive to oxygen diffusion. In the uniform convergent channel, the outlet area constantly decreases, and oxygen concentration distribution uniformity gradually becomes poor, particularly Style 8, high oxygen concentration area can only be found under the main flow channel and outermost branch channel. In addition, based on the polarization curves and the power density curves shown in Figure 9, shows the oxygen concentration distribution uniformity, and it cannot determine the output characteristics of PEMFC. Although Style 9 has the best distribution uniformity of oxygen concentration, its limiting current density and maximum power density are relatively low.

Notably, the new flow field has a higher average oxygen concentration value in the GDL/CL layer when the inlet/outlet area ratio is less than 2.5 compared with Chowdhury’s convergent serpentine flow channel [35].

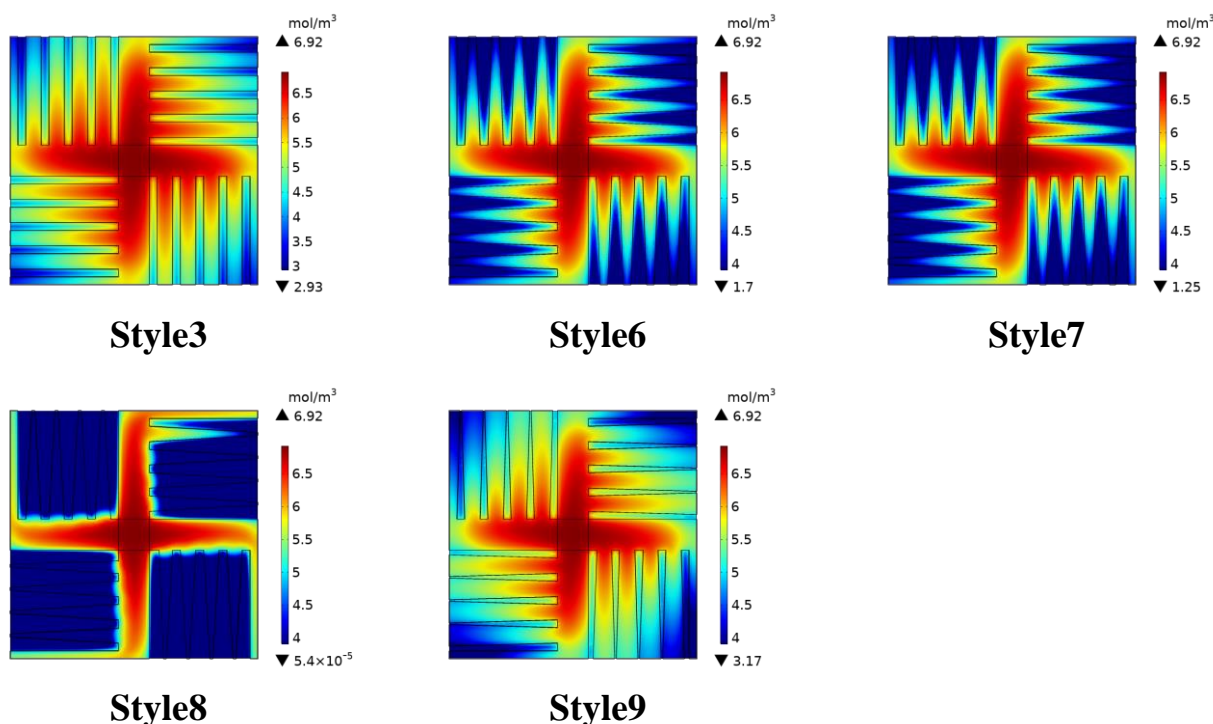


**Figure 10.** The oxygen concentration distribution of different styles in the GDL/CL layer

### 3.2.3 Influence on water content in flow channels

Figure 11 shows the water content distribution of different types of PEMFC flow channels at 0.55 V. As shown in the diagram, Style 8 shows a serious water blocking phenomenon. No water residual is found in the main flow channel, but the water content in each branch flow channel is high. As mentioned earlier, the oxygen movement rate of the uniform convergent flow channel is low, and the liquid water accumulated in the flow channel requires high-speed oxygen to carry out the flow field. Compared with Style 8, the drainage of the other four flow channels is better, and the water content in the convergent flow channel is lower than that in the divergent flow channel.

Figure 12 shows the difference of water concentration in different types of PEMFC cathode channels. The distribution is the same as that shown in Figure 11. The difference of water content

concentration in the Style 6 channel is 5.09 mol/m<sup>3</sup>, which is 10.61% lower than that in Style 3, indicating that compared with other styles of flow channels, the drainage condition of the convergent flow channel is better. Furthermore, when the inlet/outlet area ratio is 2/1, the effect of water removal is the best. After comprehensive consideration, Style 6 has the best overall performance.

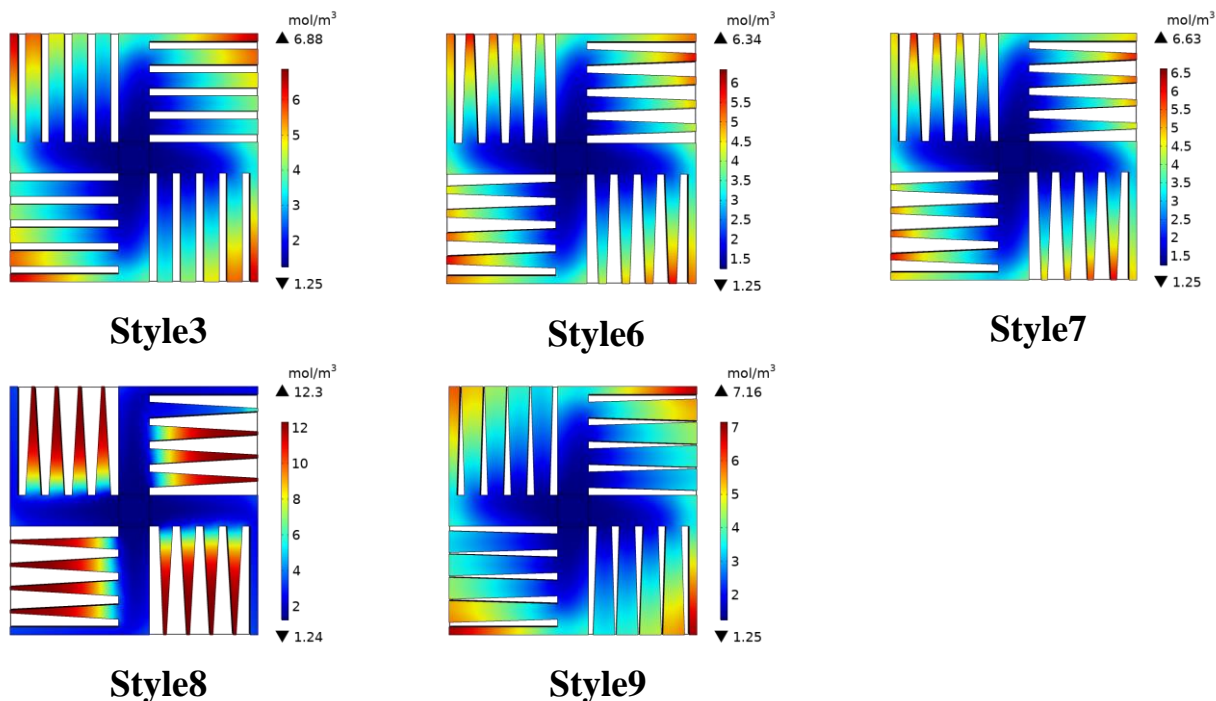


Figure 11. The water content distribution of different styles in the flow channel

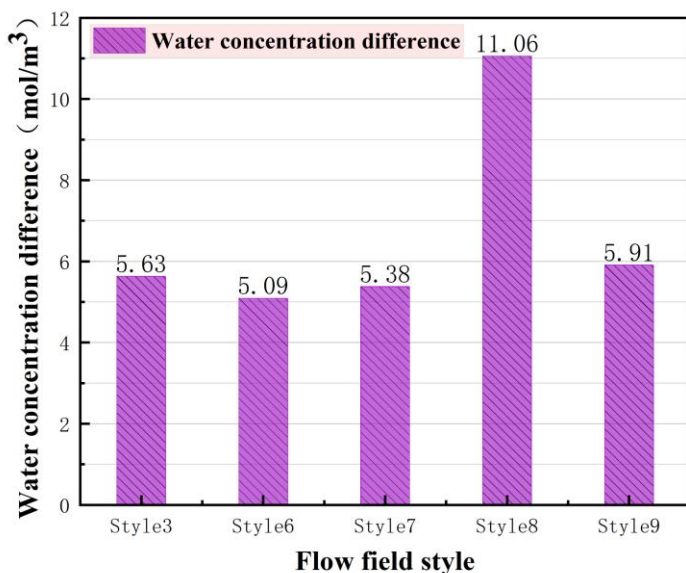
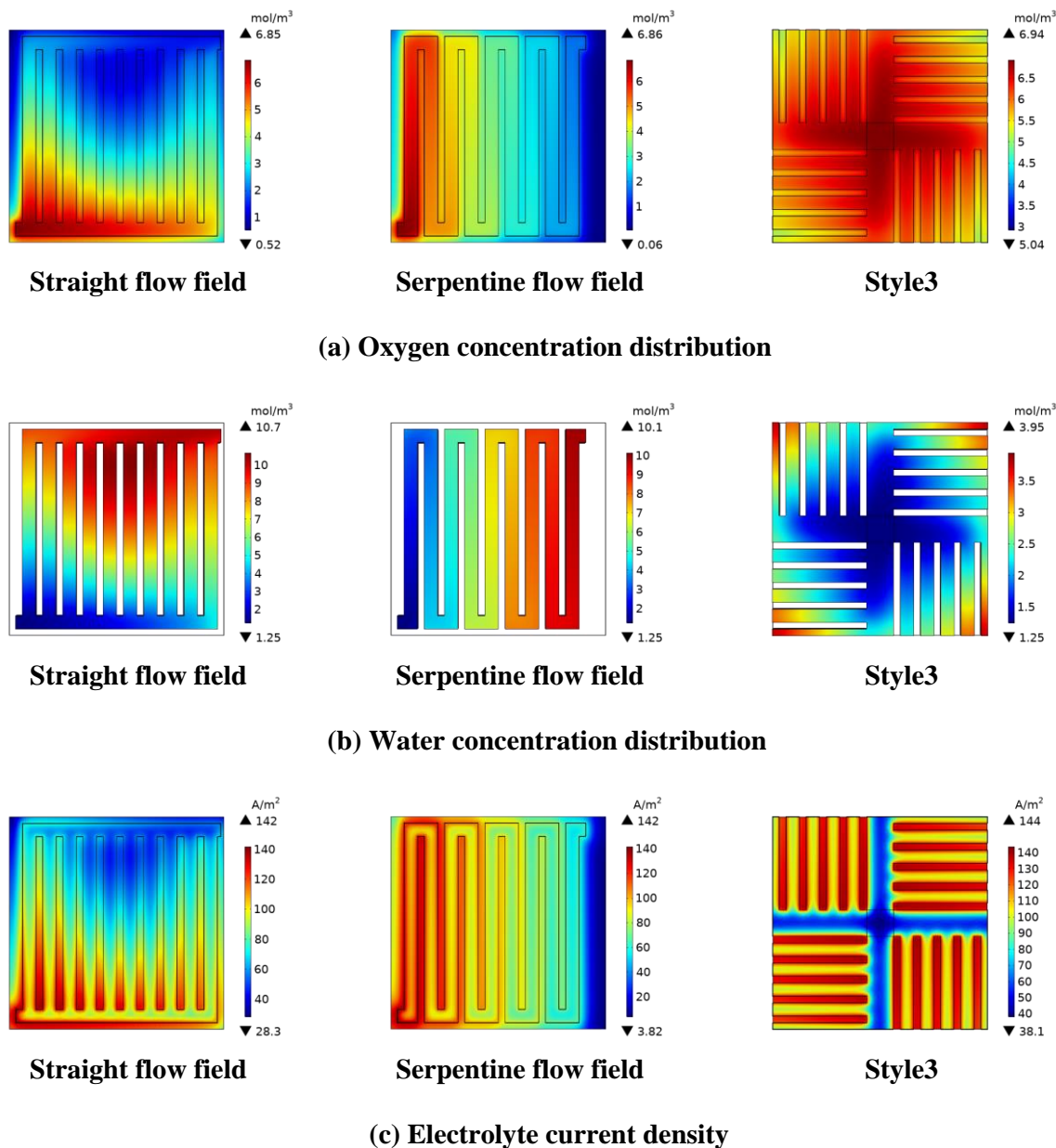


Figure 12. Difference of water concentration in different styles of PEMFC channel

### 3.2.4 Comparison with traditional flow channels

The flow channel with a rib width ratio of 2/1 has better electrochemical characteristics. At present, the parallel and serpentine fields and the improved channels based on these two types are widely

used [36]. Therefore, in ensuring the same size parameters and performance parameters, Style3 is selected and compared with the traditional parallel field and serpentine flow field to verify the advance of this structure. Figure 13 shows the distribution of oxygen concentration in the GDL/CL layer, water content in the flow field, and electrolyte current density in three different flow fields. As shown in the figure, the distribution of oxygen concentration in Style 3 is more uniform compared with the other two flow fields. Similarly, the water residue in the Style 3 flow field is lower than that in the parallel field and serpentine flow field. In addition, the electrolyte current density distribution of Style 3 is more uniform than that of the other two flow fields (Figure 13). Therefore, the reasonably designed cross inverse Z flow channel shows a better output performance.



**Figure 13.** Distribution of (a) oxygen concentration, (b) water content, and (c) electrolyte current density in three different flow fields

#### 4. CONCLUSION

In this paper, a cross inverse Z flow field is proposed, and the rib width ratio and inlet/outlet area ratio of the flow channel are considered as important research objects. Simulation analysis of the flow field is performed using CFD simulation, and their performance in oxygen concentration distribution, water concentration distribution, and other aspects is compared.

An appropriate rib width ratio can effectively improve the output characteristics of a new flow field. By comparing and analyzing the five flow field structures in this study, the new flow field shows the best comprehensive performance when the Style 3 (rib width ratio is 2/1) structure is adopted, and the limit current density and maximum power density are significantly higher than those of Styles 1, 4, and 5. Oxygen concentration distribution and water content are also in a relatively appropriate state. Although the maximum power density value is less than that of Style 2 (rib width ratio is 1/1), the pumping power consumption is lower than that of Style 2.

Under constant rib width ratio, the influence of the inlet/outlet area ratio of each branch channel on the performance of the new flow field is also studied. Although the oxygen concentration distribution of the divergent flow field is remarkable, the drainage performance is poor, and the three styles of convergent flow field can also improve this problem. The results show that appropriately increasing the cross-sectional inlet/outlet area ratio of the branch flow channel will increase the oxygen movement rate, thereby increasing the output power of the new flow field. Compared with Style 3, the maximum power density of Style 6 is increased by 1.35%. However, too small cross-sectional area at the outlet of the flow channel also results in uneven distribution of oxygen concentration and poor drainage performance, which adversely affects the output performance of PEMFC. Furthermore, Style 6 (inlet/outlet area ratio is 2/1) PEMFC has the best comprehensive performance.

#### ACKNOWLEDGMENTS

This work was supported by the Major Science and Technology Innovation Project in Shandong Province (2018CXGC0803).

#### CONFLICT OF INTERESTS

The authors declare that there are no conflicts of interest regarding the publication of this article.

#### References

1. S. Zhang, Z. Qu, and H. Xu, *Int. J. Hydrogen Energy*, 46(54) (2021) 27700-27708.
2. Z. Liao, L. Wei, A.M. DAafalla, *Int. J. Heat Mass Transfer*, 181 (2021) 121900.
3. A. Iranzo, C.H. Arredondo, A.M. Kannan, *Energy*, 190 (2020) 116435.
4. S. Pandiyan, A. Elayaperumal, N. Rajalakshmi, *Renewable Energy*, 49 (2013) 161-165.
5. S. Kreesaeng, B. Chalermssinsuwan, P. Piumsomboon. *Energy Procedia*, 79 (2015) 733-745.
6. B.H. Lim, E.H. Majlan, W.R.W. Daud, *Ionics*, 22(3) (2016) 301-316.
7. O.S. Ijaodola, Z. El-hassan, E. Ogungbemi, *Energy*, 179 (2019) 246-267.
8. J. Shen, Z. Tu, S.H. Chan, *Appl. Therm. Eng.*, 149 (2019) 1408-1418.
9. A. Mohammadi-ahmar, B. Osanloo, A. Solati, *Energy Convers. Manage.*, 128 (2016) 238-249.
10. X. Chen, Z. Yu, C. Yang, *Int. J. Hydrogen Energy*, 46(19) (2021) 11127-11139.

11. W. Zhu, M. Zheng, *Int. J. Heat Technol.*, 37(3) (2019) 733-740.
12. S.A. Atyabi, E. Afshari, *J. Cleaner Prod.*, 214 (2019) 738-748.
13. T. Monsaf, B.M. Hocine, S. Youcef, *Int. J. Hydrogen Energy*, 42(2) (2017) 1237-1251.
14. B. Kim, Y. Lee, A. Woo, *Appl. Energy*, 111 (2013) 441-448.
15. S. Shimpalee, J. Vanzee, *Int. J. Hydrogen Energy*, 32(7) (2007) 842-856.
16. M. Muthukumar, P. Karthikeyan, V. Lakshminarayanan, *Appl. Mech. Mater.*, 592-594 (2014) 1728-1732.
17. N.J. Cooper, T. Smith, A.D. Santamaria, *Int. J. Hydrogen Energy*, 41(2) (2016) 1213-1223.
18. H. Heidary, M.J. Kermani, B. Dabir, *Energy Convers. Manage.*, 124 (2016) 51-60.
19. S. Perng, H. Wu, *Appl. Energy*, 143 (2015) 81-95.
20. C. Wang, Q. Zhang, J. Lu, *Int. J. Hydrogen Energy*, 42(36) (2017) 23107-23117.
21. Korkischko. I, Carmo. B. S, Fonseca. F. C, *Fuel Cells*, 17(6) (2017) 809-815.
22. A. Ghanbarian, M.J. Kermani, *Energy Convers. Manage.*, 110 (2016) 356-366.
23. P. Karthikeyan, R.J. Vasanth, M. Muthukumar, *Int. J. Hydrogen Energy*, 40(13) (2015) 4641-4648.
24. C. Yang, Z. Wan, X. Chen, *Energy Convers. Manage.*, 228 (2021) 113651.
25. M. Rahimi-esbo, A.A. Ranjbar, A. Ramiar, *Int. J. Hydrogen Energy*, 41(4) (2016) 3023-3037.
26. N.J. Cooper, A.D. Santamaria, M.K. Becton, *Energy Convers. Manage.*, 136 (2017) 307-317.
27. K. Xiong, W. Wu, S. Wang, *Appl. Energy*, 301 (2021) 117443.
28. L. Lin, X. Zhang, H. Feng, *Sci. China Technol. Sci.*, 53(2) (2010) 453-460.
29. J. André, E. Claude, D. Sirac, *Fuel Cells*, 20(3) (2020) 231-235.
30. M. Ghasabehi, M. Ashrafi, M. Shams, *Fuel*, 285 (2021) 119194.
31. Q. Xie, *Int. J. Electrochem. Sci.*, (2021) 211057.
32. Y. Wang, Z.Y. Sun, L. Yang, *Energy Convers. Manage.*, 252 (2022) 115077.
33. Y. Lian, M. Zheng, *Int. J. Ambient. Energy*, (2021) 1.
34. J. Jang, W. Yan, H. Li, *Int. J. Hydrogen Energy*, 33(1) (2008) 156-164.
35. M.Z. Chowdhury, B. Timurkutluk, *Energy*, 161 (2018) 104-117.
36. L. Fan, Z. Tu, S.H. Chan, *Energy Reports*, 7(2021) 8421-8446.